JSTT JOURNAL OF SCIENCE AND TRANSPORT TECHNOLOGY

Journal of Science and Transport Technology
Journal homepage: https://jstt.vn/index.php/en

UNIVERSITY OF TRANSPORT TECHNOLOGY

Article info
Type of article:
Original research paper

DOI:
https://doi.org/10.58845/jstt.utt.2026.en.6.3.275-287

*Corresponding author:**
Email address:
tvkhoi.ktd@utc.edu.vn

Received: 15/08/2025
Received in Revised Form: 05/07/2026
Accepted: 15/07/2026

Direct torque control combined with extended state observer for traction motor applied in north-south high-speed railway train

An Thi Hoai Thu Anh, Tran Van Khoi*
Department of Electrical Engineering, Faculty of Electrical and Electronics Engineering, University of Transport and Communications, Vietnam

Abstract: High-speed trains are becoming increasingly popular in developing countries thanks to their ability to protect the environment and save fossil energy resources that are gradually depleting. Induction motors (IMs) are considered the first choice for traction systems for high-speed trains thanks to their high efficiency and torque-to-current ratio. To optimise the speed control performance of IMs under disturbances, the proposed direct torque control (DTC) algorithm enables direct control of motor torque and magnetic flux without a current loop. The DTC method has been proven to be an effective solution thanks to its fast response and precise control of torque and magnetic flux without the need for complex current control loops or magnetic field orientation. However, the traditional DTC method still has limitations, such as large torque ripple, current fluctuations, and difficulty controlling under rapidly changing load conditions. These limitations can cause noise and vibration and reduce the system's service life, especially in applications requiring high accuracy, such as high-speed rail trains. In addition, a load torque observer based on the Extended State Observer (ESO) is proposed to estimate the accuracy of the train's traction force under model deviation, thereby improving the operability and reliability of high-speed trains. The results show that combining the DTC and ESO provides a sound, stable motor drive system. In theory, the research results have been verified by simulation in MATLAB/Simulink using data collected from the North-South High-Speed Railway Train project in Vietnam.

Keywords: Induction motor (IM), Extended State Observer (ESO), Direct Torque Control (DTC), High-Speed Railway.

1. Introduction

Nowadays, with the development of high-speed railways, people's essential needs have changed. From there, it has advanced science and technology, helping increase the ability to maintain stability at high speeds [1]. In design and operation, it is necessary to prioritise the safety of human life and property. High-speed railways exist in many developed countries such as Japan, Germany, and China... Compared with other means of transport, such as aeroplanes, trains, and cars, high-speed railways have the following advantages: low cost, large-area operation, environmental protection, and operation in all weather conditions. The development of high-speed railways has hindered the country's transportation and industrial sectors.

Using DTC, torque is controlled as quickly as possible, significantly reducing response time and helping maintain the train's speed and accuracy during movement [2], making it optimal for controlling high-speed trains [3][4].

In a traction drive, the core transmits torque. Many problems arise even in new trains during operation due to manufacturer errors, such as the nonlinear behaviour of the transmission system [5]. Over time, these errors will cause wear and tear and consume more material [6][7]. The damage and wear of the gears cause the frequency amplitude to increase over time, leading to the gears no longer meshing. To identify problems in the transmission system, people often analyse gear and engine vibrations using conventional acceleration-measuring instruments [8][9]. However, instead of measuring complex vibrations, torque analysis calculations can also be used with observation systems [10].

Load torque is essential for monitoring the operating state and improving engine efficiency. Observing the load torque is extremely important for monitoring the engine and transmission system [11][12]. While the high-speed train is operating to determine torque transmission errors, the first step is to build a specific database and a particular waveform of the load torque for the fault-free and faulted systems. From there, error criteria are given for adequate correction, so an ESO is applied to observe the load torque [13-15]. This method has certain advantages and helps resolve some errors that occur during train operation. The ESO observes and estimates many direct impacts and errors affecting the object and reality. With high-speed trains, the ESO will help monitor the continuous changes in the load during operation [16-18]. From there, appropriate adjustments are made to ensure the train operates as stably as possible [19].

However, few high-speed trains use the ESO to observe the load torque [20][21]. Therefore, this paper will present DTC and ESO, which are well-known techniques individually; their integrated application specifically for traction motor drive systems in the context of Vietnam's North–South High-Speed Railway represents a novel contribution at the application level. The key contributions of this paper are: (1) designing DTC–ESO control suitable for the operational profile (acceleration, holding, coasting, braking) of high-speed railway traction motors; (2) an ESO-based load torque observer designed to observe time-varying disturbances and model uncertainties inherent to railway traction conditions; and (3) simulation validation using parameters derived from the North–South High-Speed Railway first - step project specifications. Finally, the accuracy of the proposed method will be demonstrated through simulation results using MATLAB/Simulink.

2. Modelling a high-speed railway train

2.1. Mathematical model of traction motor

A traction electric motor is an asynchronous motor with a direct torque control method based on the dq coordinate system. The torque generated by the motor results from the interaction between the stator magnetic field and the rotor current, and can also be expressed as the product of the stator and rotor fluxes. The mathematical description is (1) [22][23].

$$m_M = \frac{3p}{2}\frac{L_m}{L_sL_r - L_m^2}\left(\psi_r \times \psi_s\right) = \frac{3p}{2}\frac{L_m}{L_sL_r - L_m^2}\left(|\psi_r| \times |\psi_s| \sin\delta\right) \quad (1)$$

The dynamic equation of the motor is as follows:

$$m_M - m_L = \frac{J}{p}\frac{d\omega}{dt} \quad (2)$$

where ψ_s, ψ_r are the stator flux, rotor flux; δ - the angle between the stator and rotor fluxes; L_m, L_r, L_s are the mutual inductance, rotor and stator inductances; p- the number of pole pairs; J is the torque of inertia of the electric drive system and motor; m_M, m_L are the motor torque and load torque.

2.2. Forces acting on the electric train

When the train is running on the track, there are four main types of resistance: rolling resistance, frictional resistance, air resistance, and inertial forces. The frictional resistance is usually much smaller than the other components, so it will be ignored in the model.

The drag force due to slope is given by:

$$F_{grad} = m_v g \sin\alpha \tag{3}$$

in which m_v is the total mass of the train and passengers, α is the track's slope, and g is the gravitational acceleration.

The curve resistance is calculated as follows:

$$F_C = \frac{A}{R} \tag{4}$$

With A being an empirical coefficient ranging from 450 to 800. For the train object of the problem, the track gauge is R = 1435 mm, corresponding to A = 700.

The train's resistance at speeds of 200km/h to 350km/h is reduced to the basic resistance force according to mass, calculated using the Davis formula [24-26]:

$$W = A + Bv + Cv^2 \tag{5}$$

where A, B, and C are the drag coefficients provided by the manufacturer, and v is the train speed.

3. Control design

Fig. 1 is the diagram of direct torque control (DTC) for an IM motor, which directly controls torque and flux without a current loop [27][28]. At the same time, the ESO, which monitors load torque, helps accurately estimate disturbances and environmental impacts. As we can see in the diagram, two different loops correspond to the two quantities, stator flux and torque.

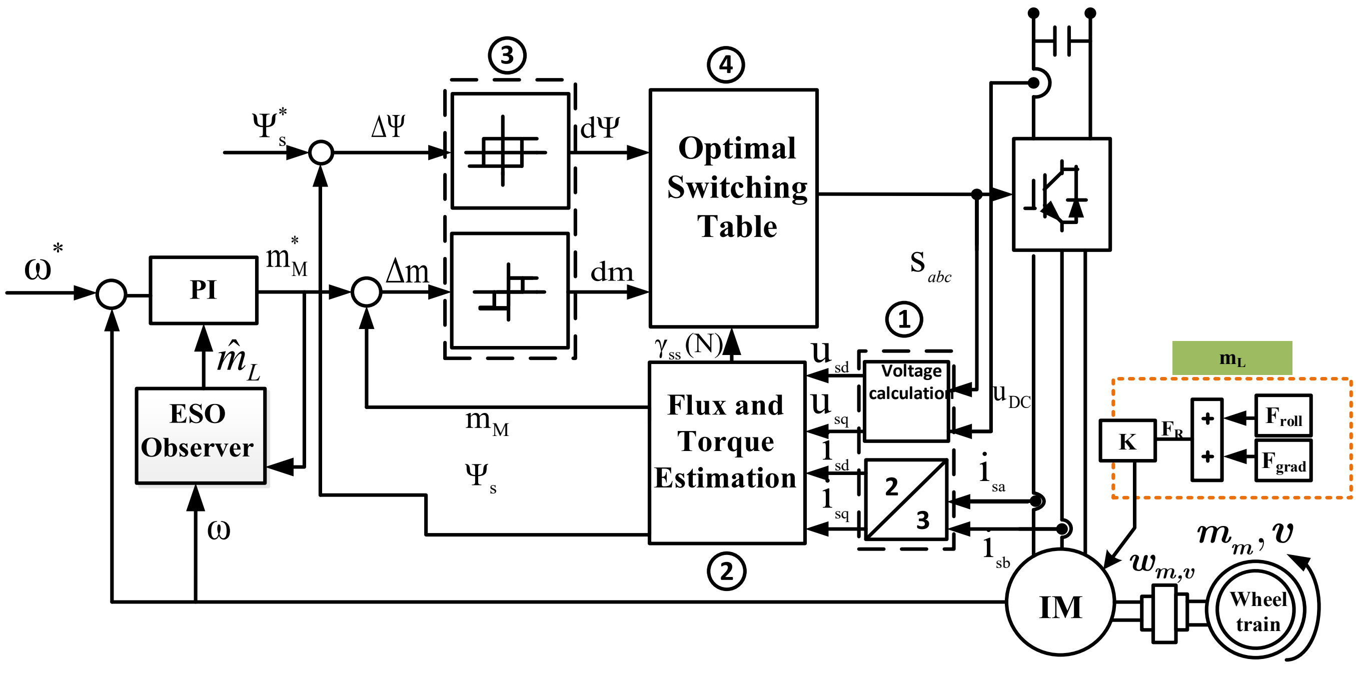

Fig. 1. DTC combined with ESO for IM

3.1. Design DTC for IM

Starting from equation (1), the motor torque is controlled by regulating the stator flux and the DTC. The DTC method directly changes the motor torque by determining the torque and flux deviations via the controllers: The torque controller with three positions and the stator flux controller with two positions, as shown in Fig. 1. Based on these deviations, the opening and closing rules of the inverter circuit valves are performed according to the optimal switching table. The DTC control law is explicitly defined as follows. The stator flux reference ψ_s^* is maintained on a circular trajectory by selecting an appropriate voltage vector $\underline{u}_s$ from the switching table (Table 1). The torque reference m_M^* is tracked by controlling the angle δ between stator and rotor flux vectors, as expressed in equation (1). At each sampling step, the hysteresis controllers compare the estimated flux ψ_s and torque m_M with their respective references and generate binary signals $d\psi \in \{0,1\}$ and $dm \in \{-1, 0, 1\}$. These signals, together with the identified stator flux sector, are used to select the optimal inverter voltage vector from Table 1, which directly and simultaneously adjusts both torque and flux. This constitutes the complete closed-loop control law of the DTC scheme.

According to equation (1), calculating stator flux:

$$\underline{\psi}_s = \int (\underline{u}_s - R_s \underline{i}_s)dt \quad (6)$$

R_s - the stator resistance; u_s, i_s- the stator voltage, current.

Since u_s remains constant at the rated value, the voltage drop across the stator resistance can be neglected, and the flux is approximately calculated as:

or $$\underline{\psi}_s = \int \underline{u}_s dt \quad (7)$$

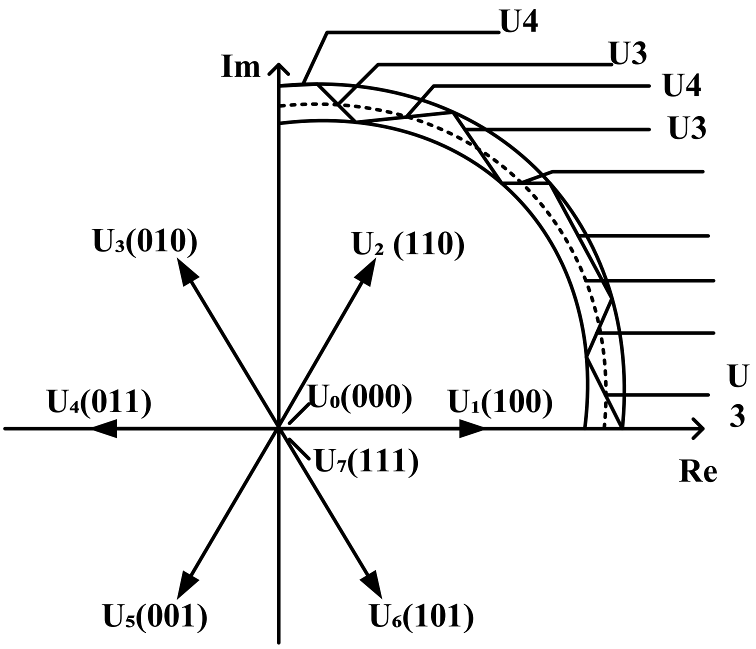

Fig. 2. Selecting the optimal voltage vector

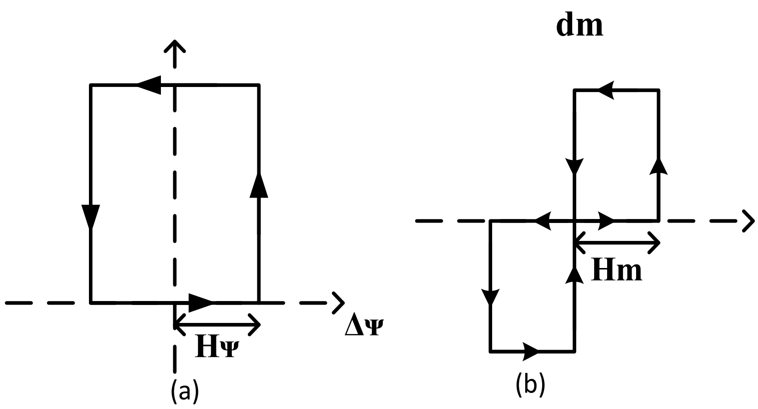

Fig. 3. Stator flux and Torque Controllers (a) Stator flux controller with two states, (b) Torque controller with three states

The stator flux amplitude varies by adjusting the voltage vector u_s, as shown in Fig. 2. The flux has only two states: increasing and decreasing, ensuring that it remains on a circular trajectory. That explains why the flux controller has only two states in Fig. 3a, while the train's operation includes acceleration, deceleration, and constant speed, corresponding to the three-state torque control in Fig. 3b.

The output signals dψ, dm are defined as:

$$\begin{cases} d\psi = 1 \Rightarrow \Delta\psi > H_\psi \\ d\psi = 0 \Rightarrow \Delta\psi < -H_\psi \end{cases} \qquad \begin{cases} dm = 1 \Rightarrow \Delta m > H_m \\ dm = 0 \Rightarrow \Delta m = 0 \\ dm = -1 \Rightarrow \Delta m < -H_m \end{cases}$$

From the output signals dψ and dm, we can adjust the estimated flux. ψ_s and estimated torque m_M as in Table 1.

3.2. Design of load torque observer using the extended state observer

Understanding each state is the key to smooth and efficient operation when controlling the system. By designing the ESO, we can monitor what cannot be observed, making the system more stable and robust.

The ESO is designed as follows [23][24]:

$$\begin{cases} \dot{\hat{x}}_1 = \hat{x}_2 + \frac{\alpha_1}{\varepsilon}(y - \hat{x}_1) \\ \dot{\hat{x}}_2 = bu + \hat{\sigma} + \frac{\alpha_2}{\varepsilon^2}(y - \hat{x}_1) \\ \hat{\sigma} = \frac{\alpha_3}{\varepsilon^3}(y - \hat{x}_1) \end{cases} \tag{8}$$

with $\hat{x}_1, \hat{x}_2, \hat{\sigma}$ is the observer state, ε > 0 is the gain, $(y - \hat{x}_1)$ is the observation error, u is the control variable, $\alpha_1, \alpha_2, \alpha_3$ are positive constants satisfying Hurwitz's law.

Table 1. Voltage vector switching board according to control requirements

dψ	dm	Sector 1	Sector 2	Sector 3	Sector 4	Sector 5	Sector 6
1	1	U_2(110)	U_3(010)	U_4(011)	U_5(001)	U_6(101)	U_1(100)
	0	U_7(111)	U_0(000)	U_7(111)	U_0(000)	U_7(111)	U_0(000)
	-1	U_6(101)	U_1(100)	U_2(110)	U_3(010)	U_4(011)	U_5(001)
0	1	U_3(010)	U_4(011)	U_5(001)	U_6(101)	U_1(100)	U_2(110)
	0	U_0(000)	U_7(111)	U_0(000)	U_7(111)	U_0(000)	U_7(111)
	-1	U_5(001)	U_6(101)	U_1(100)	U_2(110)	U_3(010)	U_4(011)

From equation (2):

$$\Rightarrow \dot{\omega} = \frac{Z_p}{J} m_M - \frac{Z_p}{J} m_L \tag{9}$$

Substituting (8), we get:

$$\begin{cases} \dot{\hat{\omega}} = \frac{Z_p}{J} m_M + \hat{\sigma} + \frac{\alpha_2}{\varepsilon^2}(\omega - \hat{\omega}) \\ \dot{\hat{\sigma}} = \frac{\alpha_3}{\varepsilon^3}(\omega - \hat{\omega}) = -\frac{Z_p}{J} m_L \Rightarrow m_L = -\frac{J}{Z_p}\frac{\alpha_3}{\varepsilon^3}(\omega - \hat{\omega}) \end{cases} \tag{10}$$

with $y = \omega;\ \hat{x}_1 = \hat{\omega};\ \hat{x}_2 = \dot{\hat{x}}_1 = \dot{\hat{\omega}};\ u = m_M$

Stability is demonstrated as follows:

Theorem 1 (Asymptotic Convergence of the ESO). Consider the ESO defined in equation (8) applied to the traction motor dynamics in equation (9). Suppose the load torque m_L and its derivative are bounded (i.e., $|m_L| \le M_1$ and $|\dot{m}_L| \le M_2$ for positive constants M_1, M_2). If the gain constants k_1, k_2, k_3 are chosen such that the matrix A in equation (12) is Hurwitz, then for any initial observation error η(0), the observation error vector $\eta(t) = [\eta_1, \eta_2, \eta_3]^T$ converges asymptotically to a neighbourhood of the origin. Specifically, there exist positive constants c_1, c_2 such that $||\eta(t)|| \le c_1 \exp(-c_2 t) ||\eta(0)|| + \varepsilon$ for some residual term ε depending on $\dot{m}_L$ and the observer gain ε. Proof:

The deviation between the actual values and the observed values is defined by the vector as follows:

$$\eta = [\eta_1 \ \ \eta_2 \ \ \eta_3]^T \tag{11}$$

where:

$$\eta_1 = \frac{x_1 - \hat{x}_1}{\varepsilon^2}, \qquad \eta_2 = \frac{x_2 - \hat{x}_2}{\varepsilon}, \qquad \eta_3 = f - \hat{\sigma}$$

Taking the derivative of the error values, we get an equation of the form:

$$\varepsilon\dot{\eta} = \bar{A}\eta + \varepsilon\bar{B}\dot{f} \tag{12}$$

with $A = \begin{pmatrix} -k_1 & 1 & 0 \\ -k_2 & 0 & 1 \\ -k_3 & 0 & 0 \end{pmatrix}$, $B = \begin{pmatrix} 0 \\ 1 \\ 0 \end{pmatrix}$

Considering the characteristic equation of matrix A:

$$|\lambda I - A| = \begin{vmatrix} \lambda + k_1 & -1 & 0 \\ k_2 & \lambda & -1 \\ k_3 & 0 & \lambda \end{vmatrix} = 0 \quad (13)$$

From equation (13), we get:

$$\lambda^3 + k_1\lambda^2 + k_2\lambda + k_3 = 0 \quad (14)$$

Suppose we choose k_1, k_2, k_3 such that A is Hurwitz. In that case, there exists a unique positive definite, symmetric matrix P that satisfies the Lyapunov function for every given positive definite, symmetric matrix Q as follows:

$$A^T + PA + Q = 0 \quad (15)$$

Choose the Lyapunov function as follows:

$$V_0 = \varepsilon\eta^T P\eta \quad (16)$$

Take the derivative V_0 to get:

$$\begin{aligned} \dot{V}_0 &= \varepsilon\dot{\eta}^T P\eta + \varepsilon\eta^T P\dot{\eta} \\ &= (\bar{A}\eta + \varepsilon\bar{B}\dot{f})^T P\eta + \eta^T P(\bar{A}\eta + \varepsilon\bar{B}\dot{f}) \\ &= \eta^T\bar{A}^T P\eta + \varepsilon(\bar{B}\dot{f})^T P\eta + \eta^T\bar{A}P\eta + \varepsilon\eta^T P\bar{B}\dot{f} \\ &= \eta^T(\bar{A}^T P + P\bar{A})\eta + 2\varepsilon\eta^T P\bar{B}\dot{f} \\ &\le \eta^T Q\eta + 2\varepsilon\|P\bar{B}\|.\|\eta\|.|\dot{f}| \end{aligned} \quad (17)$$

and

$$\dot{V}_0 \le -\lambda_{min}(Q)\|\eta\|^2 + 2\varepsilon L\|P\bar{B}\|.\|\eta\| \quad (18)$$

In there $-\lambda_{min}(Q)$ is the smallest eigenvalue of Q.

To $\dot{V}_0 \le 0$, the coefficient is selected so that it satisfies the condition:

$$\lambda_{min}(Q)\|\eta\|^2 - 2\varepsilon L\|P\bar{B}\|.\|\eta\| > 0 \quad (19)$$

Then, the observation error η will converge at the asymptote. Thus, we can prove the method's stability. From equation (17), substituting (18), we obtain $dV_0/dt \le -\lambda min(Q)||\eta||^2 + 2||P||||\eta||\cdot\delta_m$, where δm is the bound on $|\dot{m}_L|/\varepsilon$. By completing the square, $dV_0/dt \le -(\lambda min(Q)/2)||\eta||^2$ whenever $||\eta|| \ge 4||P||\delta_m/\lambda min(Q)$. This confirms that the error trajectory is ultimately bounded and converges exponentially fast to a residual set whose size is proportional to δ_m and decreases as the gain ε increases. In the ideal case, $\dot{m}_L = 0$, exponential convergence to zero is guaranteed. This completes the proof of Theorem 1.

4. Simulation results

The train and traction engine simulation parameters were collected from the North-South High-Speed Railway project, which includes 23 stations over a length of 1541 km and four phases: acceleration, holding, coasting, and braking [29], [30]. The simulation parameters are shown in Tables 2 and 3.

In Fig. 4, the speed response of the electric train clearly shows that the actual speed followed the reference speed across four stages: acceleration, holding, coasting, and braking. At the 29th to 32nd second, there was an instantaneous pulse during the high-speed transition, but it quickly followed the set speed line. This demonstrates the control method's accuracy during transitions from acceleration to holding speed and from holding speed to deceleration. There was overcorrection, but it was very small and insignificant, and it quickly returned to the set value. This shows the controller's ability to handle sudden changes during phase transitions.

In Fig. 5, we see that the maximum torque is mobilised in the accelerating range, gradually decreases during the holding phase, is 0 during the coasting phase, and is negative during the regenerative braking phase, returning energy to the grid. In Fig. 6, the power response of the traction motor during the accelerating phase from 0 to the 30th seconds reaches its maximum. Next is the phase in which the train maintains a stable speed; power consumption decreases rapidly. After the 60th second, we see that the power is 0 during the coasting phase and negative during the braking phase, indicating that energy is returned to the source at this stage.

Table 2. Parameters of high-speed train

Parameters of the train	Value	Unit
Mass of train at full load (M)	494000	kg
Number of motor (N)	8	
Maximum speed (Vmax)	350	km/h
Base speed (Vb)	320	km/h
Coefficient A	1.6	
Coefficient B	0.035	
Coefficient C	0.00095561	
Wheel diameter (Dwh)	0.84	m
Transmission ratio (i)	107/16	
Gearbox performance	0.85	
Motor performance	0.95	

Table 3. Parameters of high- speed train

Parameters	Symbol	Value
Rated power	P	510 kW
Rated voltage	U_n	2150 V
Number of pole pairs	p	2
Rotor resistance	R_s	0.028 Ohms
Stator inductance	L_r	0.027 Ohms
Rotor inductance	L_s	0.028 Ohms
Total inertia torque	J	100

Fig. 7 shows that the observed load-torque response closely matches the actual value. At times of state change, between the 34th and 40th seconds, the observed value fluctuates, but it immediately returns to the actual value within a very short period. This is a positive result because it shows that the observer has accurately and effectively estimated the torque curve.

5. Comparative discussion and validation again related to DTC-based observer studies

Several studies in the literature have combined direct torque control or related torque-loop control schemes with various types of observers to improve the robustness of induction and permanent-magnet motor drives. Table 4 summarises the observer structure, control scheme, and application domain of eight representative works, spanning railway, electric-vehicle, and general industrial traction drives, together with their key limitation relative to the DTC-ESO scheme proposed in this paper.

Compared with these works, the proposed DTC-ESO scheme offers three practical advantages for the railway traction application considered in this paper. First, unlike the sliding-mode and adaptive observers in [2] and [21], the ESO used here has a simple linear structure whose gains are selected directly from the Hurwitz condition in Theorem 1, thereby avoiding the chattering phenomenon and the extensive gain-tuning effort typically associated with sliding-mode-based designs.

Second, unlike the sensorless flux/speed observers in [1], [20], and [21], which primarily aim to remove speed or current sensors, the ESO in this paper is specifically designed to estimate the load torque disturbance, which is the dominant time-varying uncertainty in railway traction caused by passenger load, track gradient, and curve resistance, quantities that are not explicitly addressed in [1], [2], [20], or [21].

Third, unlike the MPC-ESO schemes in [27] and [28], which rely on online rolling optimisation and were validated on PMSM or ARC motors under generic operating conditions, the proposed method retains the low computational burden of conventional switching-table DTC and is parameterised using data from an actual national high-speed railway project, which gives it a more direct link to the target application.

Fourth, compared with the ESO-based speed-loop design in [31] and the sliding-mode observers used for EV and multiphase traction drives in [32] and [33], which still rely on nonlinear switching or predictive-optimisation elements and therefore retain some risk of chattering or heavier online computation, the linear ESO adopted here is combined directly with the torque loop of a conventional switching-table DTC, keeping the overall scheme simple while targeting the load-torque disturbance specifically relevant to railway operation.

It should be noted that this comparison is qualitative, based on the observer structures and control objectives reported in the cited studies, rather than a head-to-head numerical benchmark. As stated in the Conclusion, a quantitative comparison of the proposed DTC-ESO scheme against conventional DTC, FOC-based control, and the observer types summarised in Table 4, under an identical high-speed railway traction profile, is identified as future work.

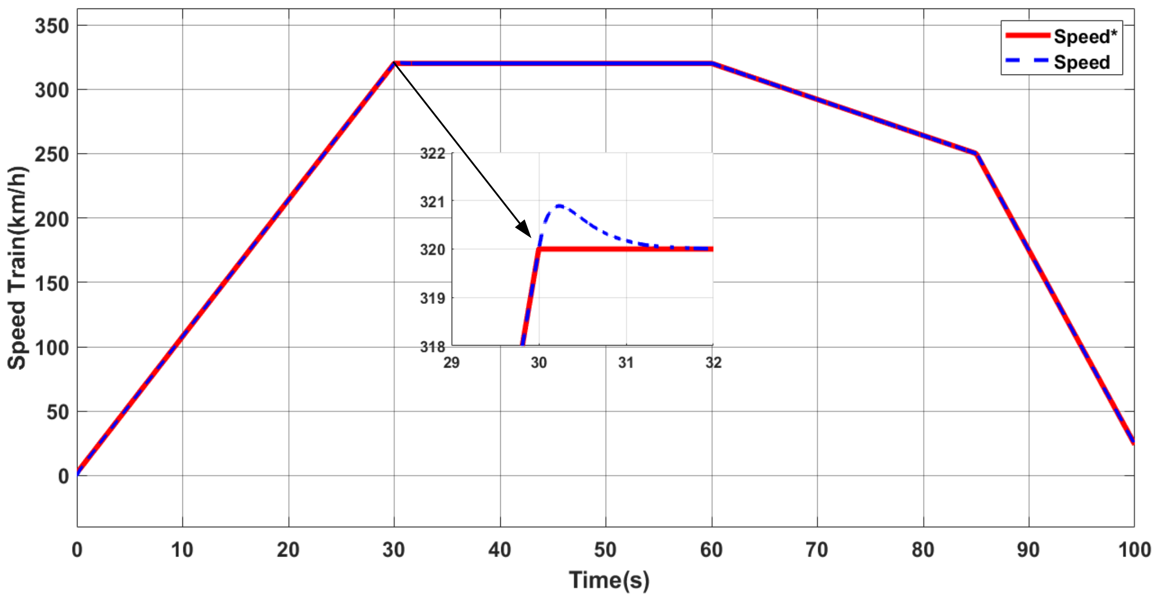

Fig. 4. Train speed curve

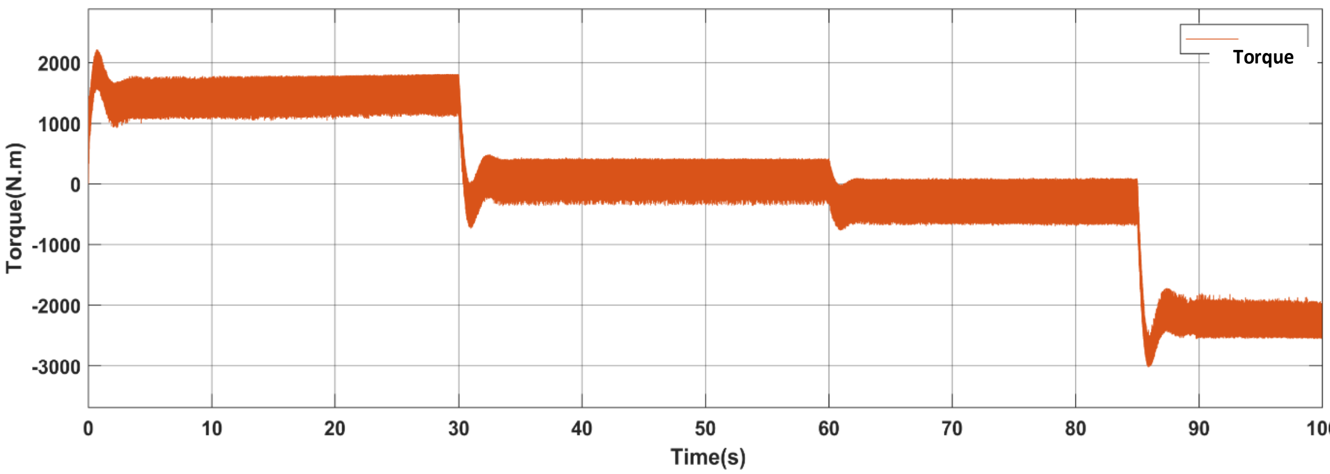

Fig. 5. Response of torque

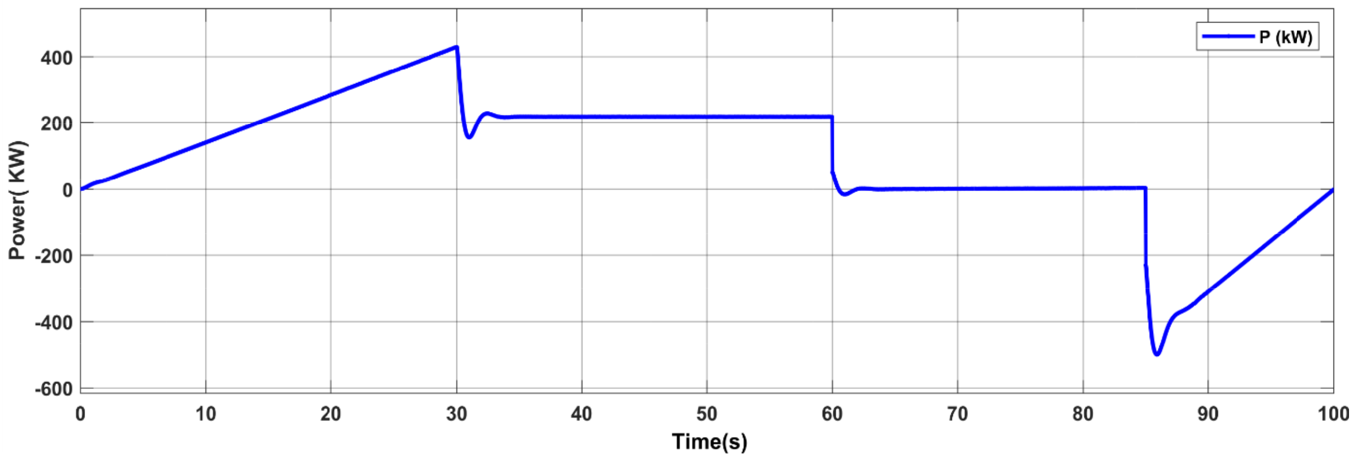

Fig. 6. Power response of the traction motor

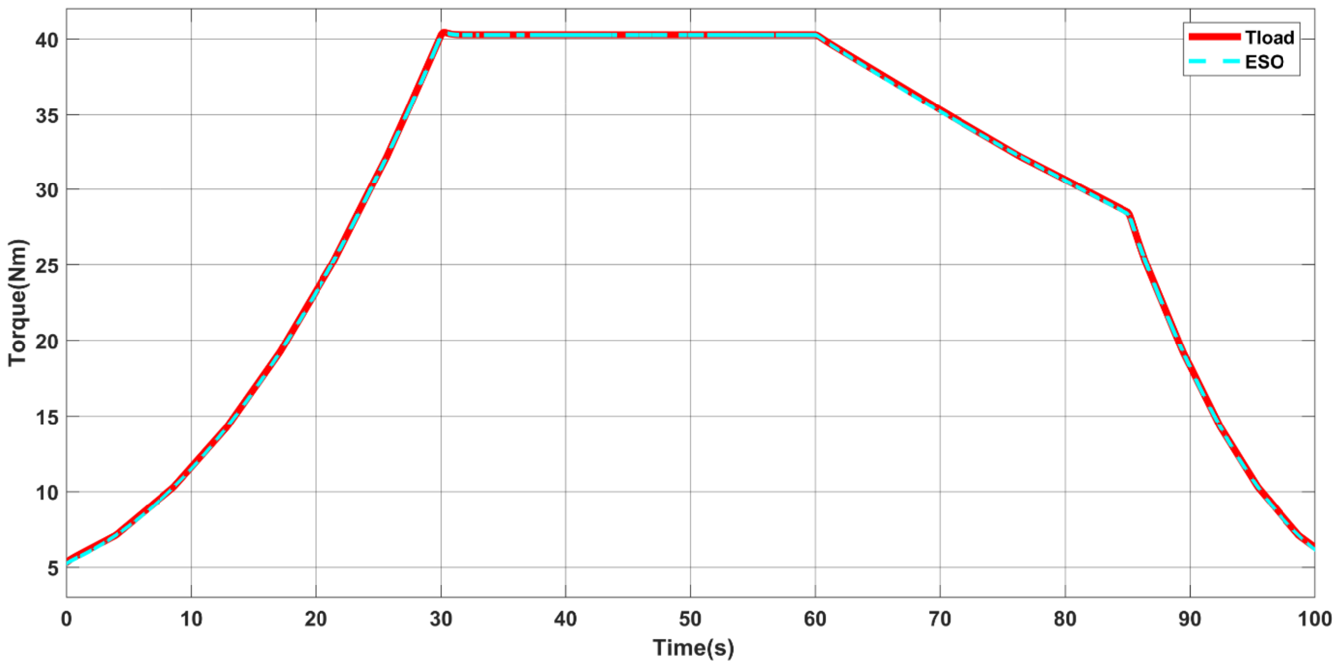

Fig. 7. Load torque observer - ESO

6. Conclusion

It can be seen that each time the train stops at stations, there will be a different number of passengers, leading to a different torque of inertia, and the A, B, and C coefficients in the David formula for the resistance forces will also differ. Furthermore, changes in weather cause deviations in the torque of inertia and the resistive force, which affect the stability of the traction motor. Therefore, this study has introduced a DTC-ESO combination to improve the stability of the traction motor drive system for long-distance high-speed railway trains. The Extended State Observer (ESO) enables estimation of load torque uncertainties. The simulation results in MATLAB/Simulink demonstrated the effectiveness of the proposed control methods for controlling the traction motor speed. It should be noted that the validation presented in this paper is based solely on simulations, using parameters derived from the North–South High-Speed Railway pre-feasibility report. Hardware-in-the-loop (HIL) testing or prototype experimentation was not conducted, and this constitutes a primary limitation of the current work. Future work will focus on: (1) quantitative comparison with conventional DTC (without ESO) and with FOC-based control to rigorously measure performance improvements in terms of torque ripple reduction, settling time, and disturbance rejection; and (2) HIL or experimental validation to further substantiate the simulation results. These steps are necessary to confirm the practical applicability of the proposed DTC–ESO scheme for real railway traction drives.

Table 4. Qualitative comparison of this study's DTC- ESO scheme with related published studies

Study	Observer type / estimated quantity	Control structure	Application domain	Limitations relative to the proposed DTC-ESO
Guzinski et al. [1], [5]	Model-based speed and load-torque observer	Field-oriented, open-loop monitoring	High-speed train electric drive	Not integrated into the torque control loop; sensitive to motor parameter accuracy.
Zhang et al. [2]	Interval sliding-mode observer (fault indicator)	Not integrated with DTC	Traction motor fault detection	Chattering and gain-tuning trade-off; not designed for real-time load-torque compensation.
Alsofyani & Idris [20]	Adaptive flux/speed estimator	Sensorless DTC	General IM drive, low-speed region	Estimates flux/speed only; load-torque disturbance not addressed; accuracy degrades near zero speed.
Yin et al. [21]	Full-order adaptive observer	Sensorless field-oriented control, low switching frequency	Railway traction (sensorless)	Coupled adaptation law increases computation; load torque not directly observed.
Liu et al. [27]; Wang et al. [28]	ESO for lumped disturbance (incl. load torque)	Model predictive control (MPC/ILC)	PMSM / ARC motor (non-railway)	Requires online rolling optimisation; not validated for railway traction load profiles.
Luo et al. [31]	Full-order adaptive sliding-mode observer + ESO	Sliding-mode speed regulation	High-speed PMSM (non-railway)	ESO paired with a nonlinear sliding-mode speed loop, not with DTC; chattering risk remains.
Kousalya et al. [32]	Sliding-mode observer	Predictive torque control	Electric-vehicle traction	SMO gain-tuning trade-off; predictive scheme needs online cost-function optimisation each step.
Shah et al. [33]	Modified sliding-mode observer	DTC with virtual voltage vectors	Six-phase induction motor drive	Reduces chattering versus classical SMO but remains a nonlinear, switching-based observer.
Proposed (this paper)	Third-order ESO, gains set from the Hurwitz condition (Theorem 1)	Hysteresis-based DTC switching table, no online optimisation	High-speed railway traction motor (Vietnam North–South HSR parameters)	Directly estimates the time-varying load torque due to passenger load and track profile, with proven Lyapunov convergence and low computational burden

Acknowledgments

This research is funded by University of Transport and Communications (UTC) under grant number T2026-DT-001.

Declaration of Generative AI

During the preparation of this work, the authors do not use Generative AI and AI-assisted technologies tools in order to generate the content of the manuscript.

References

[1]. J. Guzinski, H. Abu-Rub, M. Diguet, Z. Krzeminski, A. Lewicki. (2010). Speed and load torque observer application in high-speed train electric drive. *IEEE Transactions on Industrial Electronics*, 57(2), 565-574. doi: 10.1109/TIE.2009.2029582

[2]. K. Zhang, B. Jiang, X.-G. Yan, Z. Mao. (2019). Incipient fault detection for traction motors of high-speed railways using an interval sliding mode observer. *IEEE Transactions on Intelligent Transportation Systems*, 20(7), 2703-2714. https://doi.org/10.1109/TITS.2018.2878909

[3]. H. Chen, B. Jiang. (2020). A review of fault detection and diagnosis for the traction system in high-speed trains. *IEEE Transactions on Intelligent Transportation Systems*, 21(2), 450-465. doi: 10.1109/TITS.2019.2897583

[4]. K. Zhang, J. Yang, C. Liu, J. Wang, D. Yao. (2022). Dynamic characteristics of a traction drive system in high-speed train based on electromechanical coupling modeling under variable conditions. *Energies*, 15(3), 1202. doi: 10.3390/en15031202

[5]. J. Guzinski, M. Diguet, Z. Krzeminski, A. Lewicki, H. Abu-Rub. (2009). Application of speed and load torque observers in high-speed train drive for diagnostic purposes. *IEEE Transactions on Industrial Electronics*, 56(1), 248-256. doi: 10.1109/TIE.2008.928103

[6]. J. Xun, T. Tang, B. Ning. (2011). Optimization of speed profile for delayed train entering station. *Proceedings of 2011 IEEE International Conference on Service Operations, Logistics and Informatics*, 428-433. doi: https://doi.org/10.1109/SOLI.2011.5986598

[7]. A.N. Abdullah, M.H. Ali. (2020). Direct torque control of IM using PID controller. *International Journal of Electrical and Computer Engineering (IJECE)*, 10(1), 617-625. doi: 10.11591/ijece.v10i1.pp617-625

[8]. H. Su, K.T. Chong. (2007). Induction machine condition monitoring using neural network modeling. *IEEE Transactions on Industrial Electronics*, 54(1), 241-249. doi: 10.1109/TIE.2006.888786

[9]. G. Kamalapur, M.S. Aspalli. (2023). Direct torque control and dynamic performance of induction motor using fractional order fuzzy logic controller. *International Journal of Electrical and Computer Engineering (IJECE)*, 13(4), 3805-3816. doi: 10.11591/ijece.v13i4.pp3805-3816

[10]. R.G. Shriwastava, M.P. Thakre, K.V. Bhadane, M.S. Harne, N.B. Wagh. (2022). Performance enhancement of DCMLI fed DTC-PMSM drive in electric vehicles. *Bulletin of Electrical Engineering and Informatics (BEEI)*, 11(4), 1867-1881. doi: 10.11591/eei.v11i4.3714

[11]. A. Chikhi. (2014). Direct torque control of induction motor based on space vector modulation using a fuzzy logic speed controller. *Jordan Journal of Mechanical and Industrial Engineering*, 8(3), 169-176.

[12]. S. Massoum, A. Meroufel, A. Massoum, W. Patrice. (2021). DTC based on SVM for induction motor sensorless drive with fuzzy sliding mode speed controller. *International Journal of Electrical and Computer Engineering (IJECE)*, 11(1), 171-181. doi: 10.11591/ijece.v11i1.pp171-181

[13]. M.T. Lazim, M.J.M. Al-khishali, A.I. Al-Shawi. (2011). Space vector modulation direct torque speed control of induction motor. *Procedia Computer Science*, 5, 505-512. https://doi.org/10.1016/j.procs.2011.07.065

[14]. B.Q. Khanh, T.T. Minh, P.V. Bach. (2009). Improvement of direct torque control for asynchronous motor drives by using matrix converter (in Vietnamese). *Journal of Science and Technology of Technical Universities*, 74, 40–45.

[15]. G. Cimuca, S. Breban, M.M. Radulescu, C. Saudemont, B. Robyns. (2010). Design and control strategies of an induction-machine-based flywheel energy storage system associated to a variable-speed wind generator. *IEEE Transactions on Energy Conversion*, 25(2), 526–534. doi: 10.1109/TEC.2010.2045925

[16]. H. Maghfiroh, J.S. Saputro, F. Adriyanto, A. Sujono, R.L. Lambang. (2021). Performance evaluation of fuzzy-PID in speed control of three phase induction motor. *IOP Conference Series: Materials Science and Engineering*, 1096, 012071. doi: 10.1088/1757-899X/1096/1/012071

[17]. N.R.B. Hatem, M. Mostefai, O.E.K. Aktouf. (2019). Extended Kalman observer based sensor fault detection. *International Journal of Electrical and Computer Engineering (IJECE)*, 9(3), 1546–1552. doi: 10.11591/ijece.v9i3.pp1546-1552

[18]. S.G. Malla. (2016). A review on Direct Torque Control (DTC) of induction motor: With applications of fuzzy. *2016 International Conference on Electrical, Electronics, and Optimization Techniques (ICEEOT). IEEE*, pp. 4557-4567. doi: 10.1109/ICEEOT.2016.7755579

[19]. M. Uddin, M. Hafeez. (2011). FLC-based DTC scheme to improve the dynamic performance of an IM drive. *IEEE Transactions on Industry Applications*, 48(2), 823-831. doi: 10.1109/TIA.2011.2181287

[20]. I. Alsofyani, N. Idris. (2016). Simple flux regulation for improving state estimation at very low and zero speed of a speed sensorless direct torque control of an induction motor. *IEEE Transactions on Power Electronics*, 31, 3027-3035. doi: 10.1109/TPEL.2015.2447731

[21]. S. Yin, Y. Huang, Y. Xue, D. Meng, C. Wang, Y. Lv. (2019). Improved full-order adaptive observer for sensorless induction motor control in railway traction systems under low-switching frequency. *IEEE Journal of Emerging and Selected Topics in Power Electronics*, 7(4), 2333-2345. doi: 10.1109/JESTPE.2019.2898875

[22]. R.S. Raghunathan, H.-D. Kim, T. Setoguchi. (2002). Aerodynamics of high-speed railway train. *Progress in Aerospace Sciences*, 38(6-7), 469-514. doi: https://doi.org/10.1016/S0376-0421(02)00029-5

[23]. K. Song, T. Hao, H. Xie. (2018). Disturbance rejection control of air–fuel ratio with transport-delay in engines. *Control Engineering Practice*, 79, 36-49. doi: https://doi.org/10.1016/j.conengprac.2018.06.009

[24]. D.D. Tuan, N.D. Toan. (2020). Developing a program to calculate the unit resultant force of trains on Vietnam railways (in Vietnamese). *Transport and Communications Science Journal*, 71(8), 907–923. https://doi.org/10.47869/tcsj.71.7.3

[25]. N.V. Tiem. (2020). Speed control for the train of urban railway using fuzzy-d controller (in Vietnamese). *Transport and Communications Science Journal*, 71(6), 640–650. https://doi.org/10.25073/tcsj.71.6.1

[26]. T.V. Khoi, N.D. Khuong. (2019). Optimal planning of substations on urban railway power supply systems using integer linear programming (in Vietnamese). *Transport and Communications Science Journal*, 70(4), 264–278.

[27]. H. Liu, W. Lin, Z. Liu, C. Buccella, C. Cecati. (2022). Model predictive current control with model-aid extended state observer compensation for PMSM drive. *IEEE*

Transactions on Power Electronics, 38(3), 3152-3162. doi: 10.1109/TPEL.2022.3225626

[28]. J. Wang, D. Huang, S. Fang, Y. Wang, W. Xu. (2022). Model predictive control for ARC motors using extended state observer and iterative learning methods. *IEEE Transactions on Energy Conversion*, 37(3), 2217-2226. doi: 10.1109/TEC.2022.3159834

[29]. The National Assembly of Vietnam. (2024). Resolution No. 172/2024/QH15 on the Investment guideline for the North-South High-speed Railway Project.

[30]. B. Rochard, F. Schmid. (2000). A review of methods to measure and calculate train resistances. *Proceedings of the Institution of Mechanical Engineers, Part F: Journal of Rail and Rapid Transit*, 214, 185–199. doi: 10.1243/0954409001531306

[31]. M. Luo, Z. Yu, Y. Xiao, L. Xiong, Q. Xu, L. Ma, Z. Wu. (2023). Full-order adaptive sliding mode control with extended state observer for high-speed PMSM speed regulation. *Scientific Reports*, 13, 6200. doi: 10.1038/s41598-023-33455-x

[32]. K. V, R. Rai, B. Singh. (2022). Sliding model-based predictive torque control of induction motor for electric vehicle. *IEEE Transactions on Industry Applications*, 58, 742-752. doi: 10.1109/TIA.2021.3131973

[33]. K. Shah, A. Mansuri, R. Maurya. (2023). Modified sliding mode observer-based direct torque control of six-phase asymmetric induction motor drive. *Chinese Journal of Electrical Engineering*, 9(3), 111-123. doi: 10.23919/CJEE.2023.000026